



**HAL**  
open science

## Formation of locked-lamellar grains in a slightly hypoeutectic Al-Al<sub>2</sub>Cu alloy during thin-sample directional solidification

M Medjkoune, S Bottin-Rousseau, L Carroz, G Prévot, B Croset, J S Micha,  
S Akamatsu

► **To cite this version:**

M Medjkoune, S Bottin-Rousseau, L Carroz, G Prévot, B Croset, et al.. Formation of locked-lamellar grains in a slightly hypoeutectic Al-Al<sub>2</sub>Cu alloy during thin-sample directional solidification. 2022. hal-03777032

**HAL Id: hal-03777032**

**<https://hal.science/hal-03777032v1>**

Preprint submitted on 14 Sep 2022

**HAL** is a multi-disciplinary open access archive for the deposit and dissemination of scientific research documents, whether they are published or not. The documents may come from teaching and research institutions in France or abroad, or from public or private research centers.

L'archive ouverte pluridisciplinaire **HAL**, est destinée au dépôt et à la diffusion de documents scientifiques de niveau recherche, publiés ou non, émanant des établissements d'enseignement et de recherche français ou étrangers, des laboratoires publics ou privés.

# Formation of locked-lamellar grains in a slightly hypoeutectic Al-Al<sub>2</sub>Cu alloy during thin-sample directional solidification

M Medjkoune<sup>1</sup>, S Bottin-Rousseau<sup>1</sup>, L Carroz<sup>1,2</sup>, G Prévot<sup>1</sup>, B Croset<sup>1</sup>, J S Micha<sup>3</sup> and S Akamatsu<sup>1</sup>

<sup>1</sup>Sorbonne Université, Institut des Nanosciences de Paris, CNRS UMR 7588, 4 place Jussieu, 75005 Paris, France

<sup>2</sup>Currently at ArcelorMittal Industeel, 71201 Le Creusot, France

<sup>3</sup> Univ. Grenoble Alps, CEA-IRIG, 17 avenue des Martyrs, 38054 Grenoble Cedex 9, France

**Abstract.** We studied the formation and growth of locked-lamellar microstructures in a thin sample of a slightly hypoeutectic Al-Al<sub>2</sub>Cu alloy. The coupled-growth dynamics, including early stages and steady-state regimes, was observed optically in real time during directional solidification. The orientation of the  $\alpha$  (Al) and  $\theta$  (Al<sub>2</sub>Cu) crystals was measured ex situ in a series of eutectic grains by X-ray Laue microdiffraction. A nucleation event of a  $\theta$  crystal on a pre-existing  $\alpha$  crystal, and the subsequent growth of a eutectic grain with a type-C orientation relationship, that is, with a coincidence of  $\{123\}$ - $\alpha$  and  $\{100\}$ - $\theta$  planes, were observed in situ. In type-C eutectic grains, lamellar locking occurred parallel to the low-energy coincidence plane. A regular (*floating*) coupled-growth dynamics was observed in misoriented eutectic grains.

## 1. Introduction

Composite microstructures in solidified eutectics are a frozen trace of two-phase growth patterns at the moving solid-liquid interface [1]. During directional solidification of a nonfaceted binary eutectic alloy at an imposed velocity  $V$  in a fixed temperature gradient  $G$ , two solid phases grow simultaneously. In steady-state, they form periodic patterns, the dynamics of which is essentially determined by solute diffusion in the liquid and capillary effects. This is well described by the Jackson-Hunt (JH) theory of regular eutectics [2]. Depending on initial conditions, a coupled-growth pattern smoothly evolves towards a spatially periodic structure, or undergoes symmetry breaking instabilities leading to complex spatio-temporal phenomena [3]. Such a *floating* dynamics is typical of an isotropic system. In practice, a eutectic ingot is often composed of distinct eutectic grains –in a eutectic grain, all the crystals of each phase have the same, fixed orientation with respect to a reference frame. The eutectic-grain dependence of coupled-growth microstructures in eutectic alloys has been extensively documented since the 1970's [4]. The problem has been rigorously formalized much more recently by considering the so-called locking dynamics of tilted-lamellar patterns [5]. The central feature is that the free energy  $\gamma$  of the interphase boundary between the two solids is commonly anisotropic, and depends on the inclination angle  $\phi$  (we consider a 2D geometry) of the interphase boundary. This modifies the theoretical problem via the local equilibrium at the triple junction between the liquid and the two solids (Young-Herring equation) [6]. A marked interfacial-anisotropy effect arises in eutectic grains with an orientation relationship (OR) such that  $\gamma$  presents a deep, possibly singular minimum for an inclination corresponding to that of dense lattice planes in coincidence. Locked lamellae grow (nearly) parallel to such a low-energy plane, independently of control parameters. They can be strongly tilted with respect to the main solidification axis  $\mathbf{z}$ , by an angle  $\phi_t$  that is equal to, or close to that of the coincidence planes. A semi-empirical theory has been proposed, according to which the steady-state tilt angle  $\phi_t$  can be

calculated, on a first approach, knowing the function  $\gamma(\phi)$  and the orientation of the eutectic grain [5,7]. Recent experimental studies also shed light to the link between coincidence planes and the dynamics of lamellar patterns in anisotropic eutectic grains [8-12]. However, key information on the formation mechanisms of locked-lamellar eutectic grains during early solidification stages in well-characterized alloys, with good knowledge of both the ORs and the coupled-growth dynamics is still lacking.

We present the analysis of a thin hypoeutectic Al-Al<sub>2</sub>Cu sample slightly below the eutectic concentration (on the Al side). We combined in situ observations during directional solidification, and ex situ crystallographic analysis. This study brings several pieces of clarification that were lacking so far. First, by monitoring early stages of the solidification process, direct, unequalled evidence was given of the formation of a eutectic grain with a type-C OR (see below), starting from the nucleation of a  $\theta$  crystal onto a pre-existing  $\alpha$  one, to the growth of a locked-lamellar microstructure ( $\alpha$ : fcc Al-rich solid solution;  $\theta$ : tetragonal intermetallic Al<sub>2</sub>Cu). Second, the coexistence of several eutectic grains in a thin sample permitted to differentiate crystallographic effects, all other parameters being equal. Third, crystal orientation measurements were made, for the first time in this field, with an X-ray Laue microdiffraction (MD) method at the European synchrotron (ESRF). The MD technique delivers accurate information on the orientation of the crystals on a local scale, and permits a non-invasive mapping of the ORs in the eutectic grains on the scale of the sample, without any degradation of the metallic film.

We recall that a remarkable OR is characterized by a heteroepitaxial interphase boundary, corresponding to a pair of mutually parallel dense lattice planes of the two solids (coincidence planes), and a pair of mutually parallel dense directions (coincidence directions). Eutectic grains with the same coincidence planes, but different coincidence directions, are said to belong to a given family of ORs. In bulk Al-Al<sub>2</sub>Cu ingots, previously observed ORs were most commonly of the so-called Alpha [(001) <sup>$\alpha$</sup> //(001) <sup>$\theta$</sup> ] and Beta [(111) <sup>$\alpha$</sup> //(2-11) <sup>$\theta$</sup> ] OR families [13-15]. The type-C OR family, with {123} <sup>$\alpha$</sup>  and {100} <sup>$\theta$</sup>  coincidence planes, has been recently identified in thin hypoeutectic Al-Al<sub>2</sub>Cu alloys [11].

## 2. Methods

Details on the thin-sample directional solidification method can be found in Ref. [11]. A thin Al-Cu film was prepared by plasma sputtering on a flat single-crystal sapphire plate (also see [16]). Calibrated layers of pure Al and Cu were deposited so that the average (hypoeutectic) concentration  $C_0 = 16.85$  at% of the film (total thickness: 14.3  $\mu\text{m}$ ) after melting was slightly below the eutectic point  $C_E = 17.5$  at% (majority phase:  $\alpha$ ). The metallic film (lateral dimensions  $\approx 6 \times 50$  mm<sup>2</sup>) was designed using a mask during evaporation with a 0.45-mm wide crystal-selector channel and a V-shaped crystal expander. A second sapphire plate was sealed on top of the film. At the beginning of the experiment, the sample was placed in the DS setup, and a rapid, but partial directional melting was performed. A solid seed was left unmolten in the crystal selector channel. After a short holding time, directional solidification was started at  $V=0.5$   $\mu\text{m s}^{-1}$  along the axis  $z$  of the temperature gradient ( $G \approx 70$  Kcm<sup>-1</sup>) realized between two metallic blocks with thermal regulations. The solidification front was parallel to a planar isotherm close to the eutectic temperature  $T_E \approx 548^\circ\text{C}$ , near the middle of the 1-cm gap separating the two blocks. The structure of the contact surface between the sapphire plate and the metallic film was observed in real-time with a long-distance, reflected-light optics (and a camera). The large-scale microstructure (panorama) was reconstructed ex situ from micrographs recorded at room temperature.

The Laue MD technique was performed at the French CRG-IF BM32 beamline at ESRF [17]. In brief, a small (typically 200 $\times$ 500 nm<sup>2</sup> in size) polychromatic (5–22 keV) beam was sent to the surface of the film (with 40° incident angle). Scattering intensity patterns, so-called Laue patterns, were recorded from illuminated crystals in reflection-mode (deviation angles  $\approx 90^\circ$ ) on a planar detector. Thanks to the high synchrotron flux and X-ray penetration capability, the X-ray beam could cross twice the upper sapphire plate (previously thinned to about 200  $\mu\text{m}$  by polishing), thus avoiding any mechanical degradation of the metallic film. Regions of interest in sample (ROIs) –typically 100 $\times$ 50  $\mu\text{m}^2$ – were chosen by means of visible light microscopy (Fig. 1a). In a Laue pattern,  $\theta$  or  $\alpha$  diffraction peaks were detected along with those of the sapphire (Fig. 1b). Separate indexation of the phases was unambiguous. A raster scan of each ROI was carried out by displacing the XY stage of the sample holder with 2–3  $\mu\text{m}$  steps –

significantly smaller than the lamella width. It typically contained several hundreds of pixels, corresponding to as many Laue patterns. Simultaneously, a chemical map of the actual ROI was obtained with a fluorescence detector selecting a characteristic X-ray emission line of Cu (Fig. 1a). The good quality of the signal is evidenced in Fig. 1c: the scattering  $\theta$  diffraction peak vanishes when the X-ray beam hits an  $\alpha$  crystal, and vice versa. Hence, the optical, chemical and crystallographic maps of the  $\theta/\alpha$  alternation are in good agreement with each other. After the standard calibration geometry procedure, Laue patterns indexation was made using the LaueTools software [18] with the lattice symmetry and unit-cell parameters as input data (in addition to instrumental ones). While standard EBSD systems automatically deliver crystal-orientation maps, the analysis of the Laue diagrams was made by the operator, pixel per pixel at that time. Consequently, a few Laue patterns per lamella were analysed. The results will be presented in the form of stereographic projections.

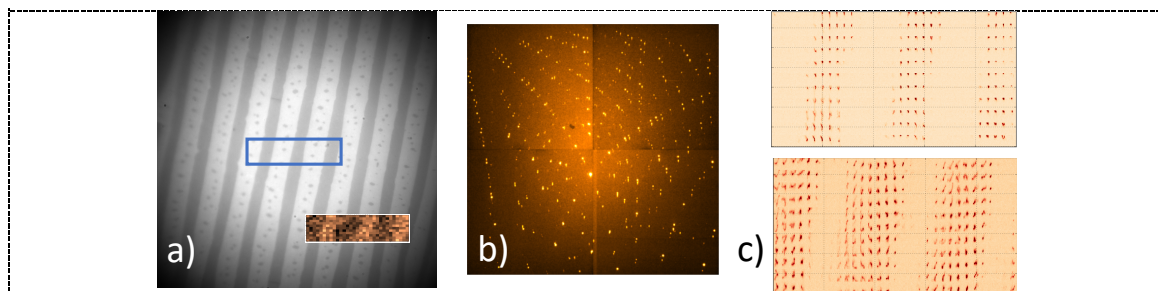


**Figure 1.** a) Optical view of the lamellar pattern in eutectic grain G6. Horizontal dimension: 200  $\mu\text{m}$ . Lamellae of the  $\theta$  ( $\alpha$ ) phase appear dark (bright) –thin  $\theta$  precipitates are visible in  $\alpha$  lamellae. Inset: fluorescence signal over the  $62 \times 22 \mu\text{m}^2$  ROI (blue frame), with (noisy) contrast peaks between Cu-rich  $\theta$  and Cu-poor  $\alpha$  regions. b) Laue MD diagram in a  $\theta$  lamella (with diffracted peaks from the sapphire plates and the  $\theta$  crystal); acquisition time : 3 s. c) Two-dimensional map of the same detector area around a peak of the  $\theta$  phase (top) and the  $\alpha$  phase (bottom).

### 3. Results

A panorama of the solidification microstructure in the crystal expander of the thin Al-Al<sub>2</sub>Cu sample is shown in Fig. 2. Representative details of the microstructures are shown in a series of insets. Most of the eutectic grains (G1 to G6), but not all of them, were oriented, as well as two majority-phase ( $\alpha$ ) dendrites along the sides of the V-shaped region (see Fig. 2, inset 1). One of the two dendrites, on the left, was an ordinary needle-like dendrite (D), while the other one, on the right, was a seaweed dendrite (SW). Both dendrites originated from two  $\alpha$  crystals in the crystal selector channel. Grains G3 and G6 exhibit a locked-lamellar microstructure, G1 and G2 a floating-like one, grain G5 weakly locked (or anisotropic floating) lamellae, and G4 an unsteady, strongly 3D pattern. An in situ snapshot of the coupled-growth pattern (grains G3, G4 and G5) is shown in Fig. 3. The analysis of representative Laue patterns are presented in Fig. 4. The choice was made to display three stereographic projections, within which the  $\{123\}^\alpha$  and  $\{100\}^\alpha$  poles of eutectic grains (and dendrites) sharing the same  $\alpha$  crystal are respectively assembled. The good  $(123)^\alpha // (100)^\theta$  coincidence in eutectic grains with a type-C OR was thus highlighted. Let us review the main features. The D dendrite was growing with the  $(101)^\alpha$  plane parallel (within  $3.4^\circ$ ) to the sample plane (Fig. 4a). The growth direction was about  $10^\circ$  off the  $[-101]^\alpha$  direction, and far away from any  $\langle 100 \rangle^\alpha$  axis. The dendrite was therefore influenced by the edge of the film. The SW dendrite was oriented with a  $(111)^\alpha$  plane nearly parallel (within about  $11^\circ$ ) to the sample plane (Fig. 4c). Incidentally, in a cubic crystal (here,  $\alpha$ ), the 4-fold anisotropy of the solid-liquid interface vanishes in a  $(111)^\alpha$  plane (3-fold symmetry). In a thin sample, the solidification dynamics is essentially two-dimensional, and needle-like dendritic growth is replaced by a seaweed morphology [19]. Both D and SW dendrites were growing ahead of the eutectic, but were hardly visible in situ because of a very thin, opaque liquid film running between the solid and the sample wall. That film was not uniform in thickness, and liquid pockets surrounded by the crystal contacting the sample wall were visible (Fig. 5). The shape of the dendrites was revealed after encapsulation by the eutectic (Fig. 2).

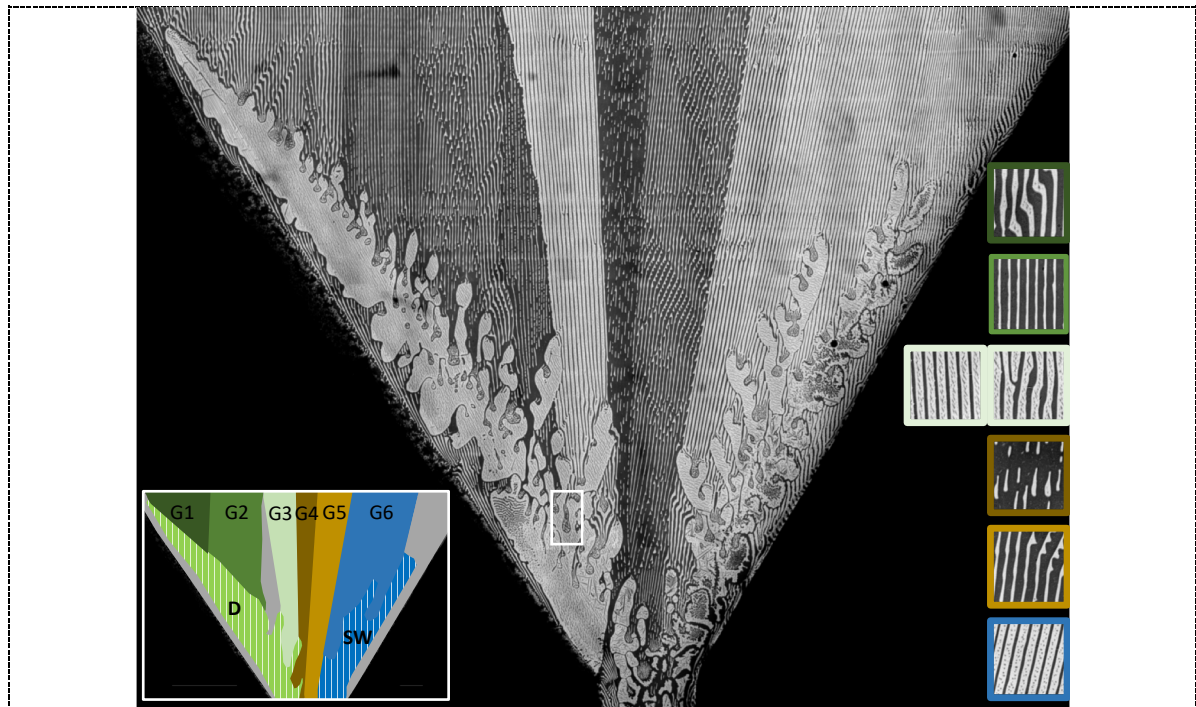


**Figure 2.** Panorama of the lamellar microstructure in a thin hypoeutectic Al-Al<sub>2</sub>Cu sample (horizontal dimension: 5.2 mm). The solidification axis was along the vertical. The  $\alpha$  ( $\theta$ ) phase appears bright (dark). The end of the crystal-selector channel can be seen at the bottom of the V-shaped crystal expander. White rectangular frame: region of the  $\theta$  nucleation event giving rise to grain G3. Inset 1 (on the left): schematic representation of the eutectic-grain structure (G1 to G6 grains were oriented; grey regions were not) and the two  $\alpha$  dendrites (D and SW). Insets (on the right): details of the microstructure (from top to bottom: G1 to G6; same color code as in Inset 1).

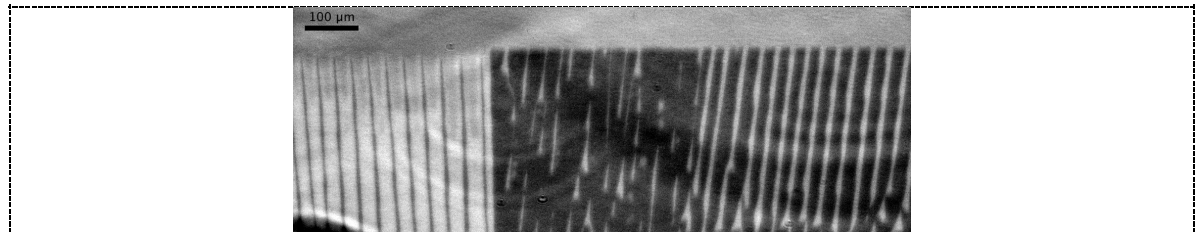


**Figure 3.** In situ optical observation of a lamellar pattern. Eutectic grains G3, G4 and G5, from left to right. The apparent variations of the volume phase fraction from one grain to another is related to 3D morphological features of the microstructure in the thickness of the film (see text).

Type-C ORs were found in eutectic grains G3 and G4. Crucially, the nucleation event that gave rise to G3 was captured in real time. In Fig. 5a, one can see the eutectic circumventing primary and secondary branches of the D dendrite. The key feature to be noticed is a shallow pocket of metastable liquid (close to the left hand edge of the image in Fig. 5a) remaining between the dendrite and the sapphire wall, isolated from nearby  $\theta$  crystals, below the eutectic temperature. A few seconds later (Fig. 5b), a  $\theta$  crystal nucleated and grew along the triple  $\theta$ -liquid-sapphire contact line. A fine eutectic microstructure rapidly formed, giving rise to grain G3 during further solidification. In this grain, lamellar locking occurred in the vicinity of the  $(123)^\alpha // (100)^\theta$  coincidence plane, in agreement with Ref. [11]. The coincidence plane was, however, not perpendicular to the sample walls (Fig. 4a). This is thus a typical case of “out-of-plane” locking close to a deep  $\gamma$  minimum: the interphase boundaries are inclined in the thickness of the sample [5]. There is obviously a limit inclination angle for stable out-of-plane locking to occur. This is



evidenced in grain G4 (which formed in the crystal selector channel). In that grain, the out-of-plane  $(123)^\alpha // (100)^\theta$  coincidence plane (inclined by an angle of about  $35^\circ$ ) was clearly unavailable for steady-state locking. Instead, a complex, unsteady growth, with marked deformations of the interphase boundaries occurred in the thickness of the sample, thus indicating a strong interfacial-anisotropy effect.

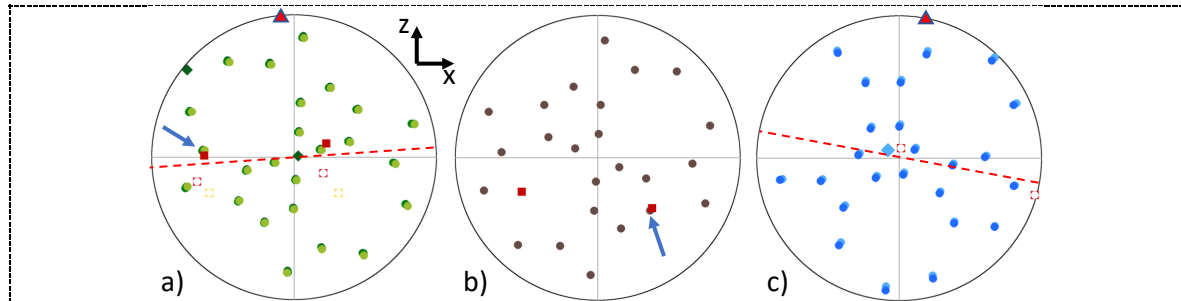


**Figure 4.** Stereographic projections (central pole: normal to the sample plane) of local crystal orientations obtained by Laue microdiffraction. Disks:  $\{123\}^\alpha$  poles (same color code as in Fig. 2, inset 1). Filled (empty) squares:  $\{100\}^\theta$  planes with (without) good coincidence with a  $\{123\}^\alpha$  plane. a) G1, G2, G3 and dendrite D; b) G4 (grain G5: not shown); c) G6 and dendrite SW. Arrows: coincidence planes (G3 and G5). Triangles and dashed lines: direction of the lamellae and ensemble of possible locking planes (G3 and G6). Diamonds: a) planes  $(101)^\alpha$  and  $(-101)^\alpha$  of the D dendrite; c)  $(111)^\alpha$  plane of the SW dendrite. Directions in coincidence are not shown for clarity.

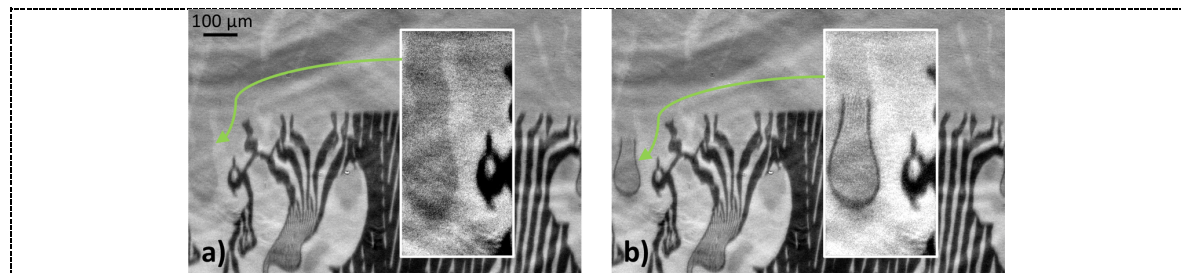


**Figure 5.** Real-time images (also see Fig. 2). a) On the very left edge of the image a thin liquid pool (with a slightly darker contrast than the surrounding  $\alpha$  solid) is enclosed between the sapphire plate and the (hardly visible) D dendrite. b) Nucleation of a  $\theta$  crystal in the liquid pool leading to the creation of grain G3. Also see the large-magnification insets. Time lapse: 4 s.

No remarkable ORs were found in other (misoriented) grains. They formed from  $\alpha$  and  $\theta$  crystals which did not nucleate one onto the other. The tilted-lamellar pattern in grain G6 is worth considering. The  $\alpha$  lamellae originated from the SW dendrite (Fig. 4c). The orientation of the  $\theta$  crystal was such that the  $(100)^\theta$  plane was closely perpendicular to the sample walls (to within less than  $1^\circ$ ). The lamellae were locked close to that plane. This, again, agrees well with the conclusion in Ref. [11] that, in misoriented grains, the lamellae can lock onto a  $(100)^\theta$  plane, whatever the orientation of the  $\alpha$  crystal relative to  $\theta$ . In the other misoriented grains, the  $\gamma$  minimum associated to the nearest  $(100)^\theta$  plane was not deep enough to stabilize an out-of-plane locking. Instead, the lamellae were growing essentially along the main solidification axis ( $\phi_r=0$ ), thus falling in a nearly isotropic part of  $\gamma(\phi)$ . The dynamics, including solitary waves, was typically floating –with a smoothly anisotropic behavior in grain G5.

Let us finally comment on the apparent variation of the volume phase fraction in the solid from one eutectic grain to another. On the basis of previous observations in bulk (near-)eutectic Al-Al<sub>2</sub>Cu ingots [12], an approximate 50/50 volume phase fraction was expected. Here, this was essentially the case in grains with a floating dynamics, and interphase boundaries perpendicular to the sample walls. Differences in grains with an out-of-plane locking dynamics is probably due to deformations of the interphase boundaries close to their contact line with the sample walls.

## 4. Conclusion

Real-time observations during directional solidification of a thin sample of a hypoeutectic Al-Al<sub>2</sub>Cu alloy provided a direct confirmation that eutectic grains with type-C ORs form from the nucleation of a  $\theta$  crystal on a pre-existing  $\alpha$  crystal. As in Ref. [11], no ORs belonging to the Alpha and Beta families were found. In the multi-grain structure of the thin sample, it also appeared clearly that steady-state lamellar locking occurred on the (123) <sup>$\alpha$</sup> //(100) <sup>$\theta$</sup>  coincidence plane in type-C grains, and on a (100) <sup>$\theta$</sup>  plane in misoriented grains, as long as out-of-plane locking was permitted by a strong anisotropy. In other cases, the lamellar growth was either anisotropic, but unsteady, or exhibited a floating dynamics. Similar investigations remain to be made in thin hypereutectic Al-Al<sub>2</sub>Cu samples with  $\theta$  as a majority phase, aiming at establishing whether a (reverse)  $\alpha$ -on- $\theta$  nucleation scenario can lead to the formation of eutectic grains with Alpha and Beta ORs.

Laue microdiffraction was employed for the first time in this research field. This non-invasive method allowed us to determine the orientation of  $\theta$  and  $\alpha$  crystals on a local scale, and to identify the ORs in distinct eutectic grains. A comparison between a comprehensive Laue microdiffraction analysis and EBSD measurements in a reference sample will be presented in a separate publication. Finally, further experimental information on the anisotropy of the interphase boundaries should be obtained via the so-called rotational directional solidification method [20,21].

## 5. References

- [1] Dantzig J A and Rappaz M 2009 *Solidification* (EPFL Press, Lausanne)
- [2] Jackson K A and Hunt J D 1966 *Trans. Metall. Soc. AIME* **236** 1129
- [3] Akamatsu S and Plapp M 2016 *Curr. Opin. Solid St M* **20** 46
- [4] Hogan L M, Kraft R W and Lemkey F D 1971 *Adv. Mater. Res.* **5** 83
- [5] Akamatsu S, Bottin-Rousseau S, Şerefoğlu M and Faivre G 2012 *Acta Mater.* **60** 3199
- [6] Hoffmann D W and Cahn J W 1972 *Surf. Sci.* **31** 368
- [7] Ghosh S, Karma A, Plapp M, Akamatsu S, Bottin-Rousseau S and Faivre G 2019 *Acta Mater.* **175** 214
- [8] Akamatsu S, Bottin-Rousseau S, Şerefoğlu M and Faivre G 2012 *Acta Mater.* **60** 3206
- [9] Kokotin V and Hecht U 2014 *Comput. Mater. Sci.* **86** 30
- [10] Bottin-Rousseau S, Senninger O, Faivre G and Akamatsu S 2018 *Acta Mater.* **150** 16
- [11] Bottin-Rousseau S, Medjkoune M, Senninger O, Carroz L, Soucek R, Hecht U and Akamatsu S 2021 *J. Cryst. Growth* **570** 126203
- [12] Hecht U, Eiken J, Akamatsu S and Bottin-Rousseau S 2019 *Acta Mater.* **170** 268
- [13] Bonnet R and Durand F 1973, in *Proceedings of the Conference on in Situ Composites* **1** 209
- [14] Hecht U, Witusiewicz V and Drevermann A 2012 *IOP Conference Series: Mat Sci Eng* **27** 012029
- [15] Wang S J, Liu G, Wang J and Misra A 2018 *Mater. Charact.* **142** 170
- [16] Sullivan E J, Tomko J A, Skelton J M, Fitz-Gerald J M, Hopkins P E and Floro J A 2021 *J. Alloy. Compd.* **865** 158800
- [17] Ulrich O, Biquard X, Bleuët P, Geaymond O, Gergaud O, Micha J S, Robach O and Rieutord F 2011 *Rev. Sci. Instrum.* **82** 033908
- [18] <https://gitlab.esrf.fr/micha/lauetools/>
- [19] Akamatsu S, Faivre G and Ihle T 1995 *Phys. Rev. E* **51** 4751
- [20] Akamatsu S, Bottin-Rousseau S, Şerefoğlu M and Faivre G 2012 *Acta Mater.* **60** 3206
- [21] Mohagheghi S and Şerefoğlu M 2019 *Metall. Mater. Trans. A* **50A** 5221

## Acknowledgments

We thank R. Soucek and L. Becerra for technical help. This work was financially supported by ANPHASES M-ERA.NET project (ANR-14-MERA-004). We also are grateful to CNES for giving us the possibility of a long-term research.